Instrument Science Report WFC3 2012-001

Proposal 11923-UVIS Filter Wedge Check

E. Sabbi
January 05, 2012

ABSTRACT

Variations in the thickness of a filter modify the distribution of the light beam, causing an apparent displacement of the observed sources. Proposal 11923 was designed to check the coplanarity (wedge) of the WFC3/UVIS spectral elements and evaluate the impact on the astrometry. We have measured the displacement of stellar positions in the 42 full-frame imaging filters. For 36 of the 42 filters the positional offset is less than 0.5 pixels. The filters that show an offset larger than 0.5 pixels are F600LP, F631N, F645N, F656N, F775W, and F850LP, with F600XP and F775W causing a shift larger than 1.0 pixels.

Introduction

The specifications for the manufacture of the UVIS and the IR filters were based on scientific and optical design requirements and are described in detail in the JPL document Specification Document D-18189. The WFC3 SOC recommended the central wavelengths and pass bands, while additional CEI specifications were developed to ensure inclusion of desired spectral features within the band-pass while avoiding undesirable spectral lines.

The two faces of a filter might be not coplanar (filter wedge) because of variations in its thickness. The wedge can introduce an offset in the position of astronomical sources with the respect of other filters and this may affect those astronomical investigations that are sensitive to the relative motion of targets within multiple filters.

During Cycle 17 the WFC3 team designed two twin proposals (11913 for the IR channel and 11923 for the UVIS channel; P.I. Mackenty) to identify which filters are affected by wedge and evaluate the impact on astrometry. Results for the IR channel have

been presented in Sabbi et al. (2010). Here we report results obtained for the 42 UVIS full-frame imaging filters. Data are presented in Section 2, the analysis is described in section 3 and results are discussed in section 4.

2. Data

The UVIS Channel of WFC3 is equipped with a selectable optical filter assembly (SOFA), made of 12 filter wheels that house 42 full frame filters, 5 quad filters and one low-resolution grism. Each wheel hosts 4 filters and has an empty slot (Fig. 1). During an observation with the UVIS channel, the wheel with the selected filter is rotated until the filter is in the light path. The other 11 wheels are rotated to put the empty slot in the light path. More information about the SOFA can be found in Dressel (2010).

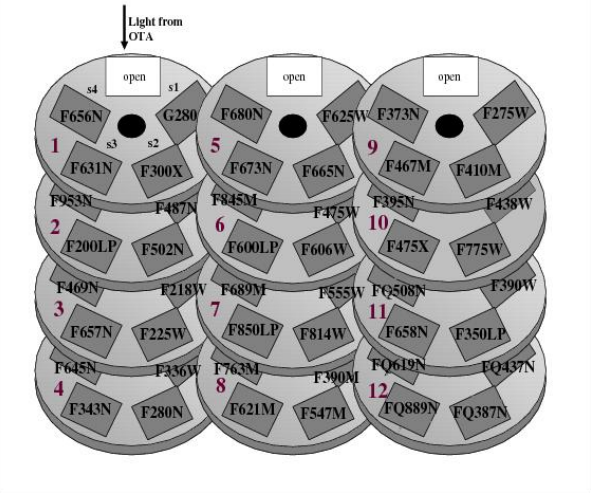

Fig. 1: UVIS Filter Wheels (Dressel 2010)

To check if any of the UVIS filters are wedged we observed the young star cluster NGC1850 (R.A.$_{J2000}$=05^{d}08^{m}41.5^{s}, Dec$_{J2000}$=-68º45'43.3") in the Large Magellanic Cloud with all the UVIS (proposal 11923) and IR (proposal 11913) filters. The cluster was selected because of its low extinction, the relatively low crowding and the richness of bright red and blue stars that makes it a suitable target for both the UVIS and IR channels. A study of the IR filter wedge has been presented in Sabbi et al (2010).

To minimize the read-out overheads, all data were acquired in a user-defined 1024x1024 sub-array placed on the upper left corner of amp A. All the full frame filters were observed in two consecutive orbits.

Since the broadband filter F606W is the reference filter for the astrometric solution of the UVIS channel (Kozhurina-Platais et al. 2009), the reference images used to measure the positional displacements of the stars in the various filters were also observed in the F606W filter (image ibch01tqq_flt.fits in the first orbit and image ibch01ugq_flt.fits in the second orbit respectively). Uncertainties introduced by movements of the telescope caused, for example, by the (re)-acquisition of the guide star, and/or by the telescope drifting (see Gilliland 2005 for more details) were taken into account by observing the cluster through the F606W filter also at the end of each orbit (images ibch01udq_flt.fits and ibcha1vuq_flt.fits respectively). This observing strategy allowed us to verify that the

telescope was correctly tracking the target during the entire orbit. The log of the observation is shown in Table 1.

Image Name	Date Obs.	Time Obs.	Filter	Exp. Time
ibch01tqq	14/07/10	13:08:10	F606W	1
ibch01trq	14/07/10	13:10:07	F300X	3
ibch01tsq	14/07/10	13:12:00	F631N	37
ibch01ttq	14/07/10	13:14:27	F656N	155
ibch01tuq	14/07/10	13:19:07	F487N	26
ibch01tvq	14/07/10	13:21:23	F502N	22
ibch01twq	14/07/10	13:23:35	F200LP	1
ibch01txq	14/07/10	13:25:24	F953N	204
ibch01tzq	14/07/10	13:30:51	F218W	28
ibch01u0q	14/07/10	13:33:09	F225W	8
ibch01u1q	14/07/10	13:35:07	F657N	20
ibch01u2q	14/07/10	13:37:17	F469N	33
ibch01u3q	14/07/10	13:39:55	F336W	3
ibch01u4q	14/07/10	13:41:48	F280N	104
ibch01u5q	14/07/10	13:45:22	F343N	7
ibch01u6q	14/07/10	13:47:19	F645N	27
ibch01u7q	14/07/10	13:49:51	F625W	2
ibch01u8q	14/07/10	13:51:43	F665N	18
ibch01u9q	14/07/10	13:53:51	F673N	21
ibch01uaq	14/07/10	13:56:02	F680N	7
ibch01ubq	14/07/10	13:58:14	F475W	1
ibch01ucq	14/07/10	14:00:02	F600LP	1
ibch01udq	14/07/10	14:01:44	F606W	1
ibch01ugq	14/07/10	14:42:03	F606W	1
ibch01uhq	14/07/10	14:43:51	F845M	8
ibch01uiq	14/07/10	14:46:04	F555W	1
ibch01ujq	14/07/10	14:47:55	F814W	2
ibch01ukq	14/07/10	14:49:47	F850LP	9
ibch01ulq	14/07/10	14:51:46	F689M	4
ibch01umq	14/07/10	14:53:55	F390M	6
ibch01unq	14/07/10	14:55:51	F547M	3
ibch01uoq	14/07/10	14:57:44	F621M	3
ibch01upq	14/07/10	14:59:37	F763M	5
ibch01uqq	14/07/10	15:01:47	F275W	6
ibch01urq	14/07/10	15:03:43	F410M	6
ibch01usq	14/07/10	15:05:39	F467M	6
ibch01utq	14/07/10	15:07:35	F373N	39
ibch01uuq	14/07/10	15:10:19	F438W	2
ibch01uvq	14/07/10	15:12:11	F775W	3
ibch01uwq	14/07/10	15:14:04	F475X	1
ibch01uxq	14/07/10	15:15:55	F395N	15
ibch01uyq	14/07/10	15:18:15	F390W	2
ibch01uzq	14/07/10	15:20:07	F350LP	1
ibch01v0q	14/07/10	15:21:58	F658N	87
ibch01v1q	14/07/10	15:25:24	F606W	1
ibch01v4q	14/07/10	16:17:47	FQ508N	12

ibch01v5q	14/07/10	16:20:03	FQ437N	54
ibch01v6q	14/07/10	16:22:46	FQ387N	47
ibch01v7q	14/07/10	16:25:22	FQ889N	106
ibch01v8q	14/07/10	16:28:57	FQ619N	34
ibch01v9q	14/07/10	16:31:32	F606W	1
ibch01vaq	14/07/10	16:33:22	FQ674N	186
ibch01vbq	14/07/10	16:38:32	FQ378N	15
ibch01vcq	14/07/10	16:40:36	FQ492N	13
ibch01vdq	14/07/10	16:42:38	FQ937N	170
ibch01veq	14/07/10	16:47:17	FQ750N	60
ibch01vfq	14/07/10	16:50:18	F606W	1
ibch01vgq	14/07/10	16:51:51	F606W	1
ibch01vhq	14/07/10	16:53:49	G280	600
ibcha1vjq	14/07/10	17:55:22	FQ672N	132
ibcha1vkq	14/07/10	17:59:36	FQ243N	205
ibcha1vlq	14/07/10	18:04:48	FQ436N	40
ibcha1vmq	14/07/10	18:07:17	FQ924N	153
ibcha1vnq	14/07/10	18:11:39	FQ727N	54
ibcha1voq	14/07/10	18:14:34	F606W	1
ibcha1vpq	14/07/10	18:16:24	FQ575N	111
ibcha1vqq	14/07/10	18:20:17	FQ232N	300
ibcha1vrq	14/07/10	18:27:04	FQ422M	14
ibcha1vsq	14/07/10	18:29:07	FQ906N	50
ibcha1vtq	14/07/10	18:31:46	FQ634N	30
ibcha1vuq	14/07/10	18:34:17	F606W	1

Table 1: Log of the observations. The first column gives the file names, date and starting time of observations are given in columns 2 and 3. Column 4 reports the filters used, while exposure times, in seconds, are provided in column 5.

3. Data Analysis

The dataset was retrieved from the Multimission Archive at Space Telescope (MAST) and re-processed with the version 2.0 of the standard calibration pipeline CALWF3 using the most up-to-date versions of bias, dark, and flat-field files. For each image the position of the stars was measured using DAOPHOT in IRAF: first in each image the sources were identified using DAOFIND, and then aperture photometry was performed using PHOT. In each image the position of the detected sources was refined via PSF-fitting with ALLSTAR by using an empirical PSF made from ~10 well isolated stars. Fig. 2 shows an atlas of the empirical PSFs as a function of wavelength. The photometric error, an estimate of the source sharpness, and the χ^2 of the PSF residuals were used to discard non-stellar objects such as cosmic rays, blended stars, background galaxies etc. In each filter we considered as *bona fide* stars only those objects that differ less then 3σ from the mean value in all of the three parameters (Fig. 3).

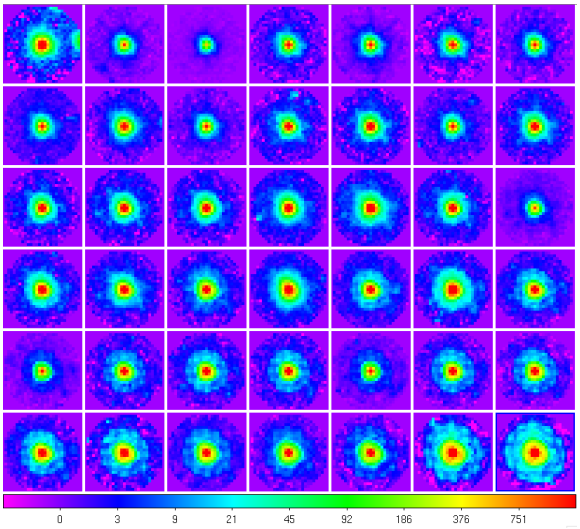

Fig. 2: From left to right, from top to bottom, atlas of UVIS PSFs in the filters F200LP, F218W, F225W, F275W, F280N, F300X, F336W, F343N, F350LP, F373N, F390M, F390W, F395N, F410M, F438W, F467M, F469N, F475W, F475X, F487N, F502N, F547M, F555W, F600LP, F606W, F621M, F625W, F631N, F645N, F656N, F657N, FF658N, F665N, F673N, F680N, F689M, F763M, F775W, F814W, F845M, F850LP, F953N

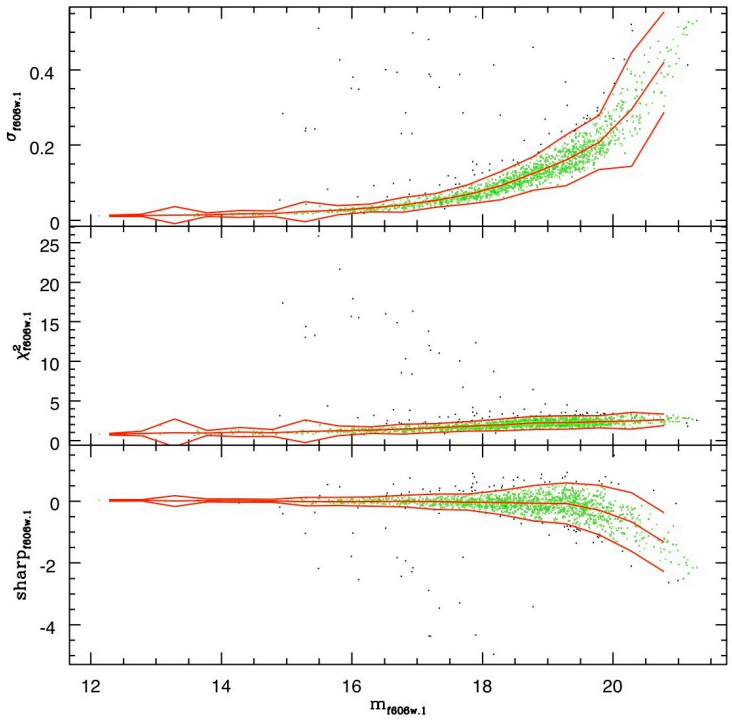

Fig. 3: Photometric error, χ^2 and sharpness of all the objects detected in the first F606W image. Objects that differ less then 3σ from the median of the distribution are plotted in green. Red lines indicate the median and the 3σ.

For each filter, individual stars where matched to those found in the reference image (ibch01tqq_flt.fits and ibch01ugq_flt.fits respectively) to measure the average shift.

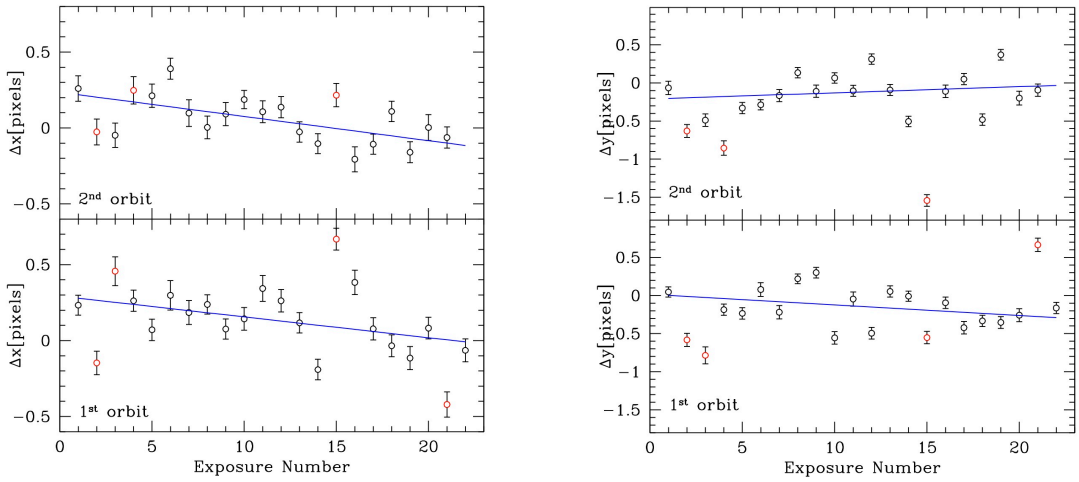

Fig. 4: Shifts along the X (left panels) and the Y (right panels) axes in pixels. The blue line marks the best fit. Filters that show a total positional displacement larger than 0.5 pixels are marked in red.

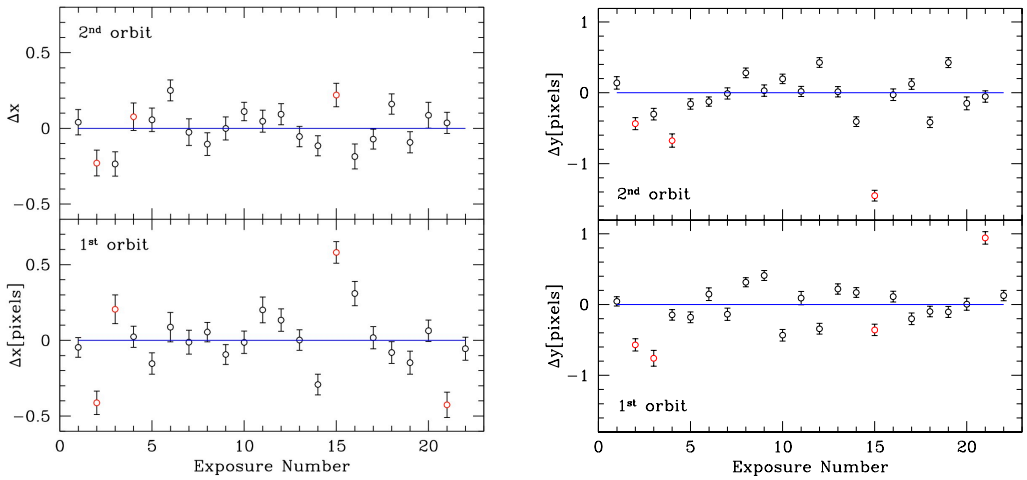

Fig. 5: The same as Fig. 4 once the correction for telescope drifting has been applied.

Fig. 4 shows an increasing offset in time, more evident toward the x direction (left panels). The average total offset from the beginning to the end of the orbit is at the level of 8 mas, consistent with the drift of the telescope, when this is operated in 3-gyro guiding mode (Gilliland 2005). A last mean square filter (highlighted by the blue line in the four panels of Fig. 4) was applied to take into account the effect of the telescope

drifting in our estimate of positional offsets introduced by the various filters. Shifts along the X and Y direction after the correction for the telescope drift are shown in Fig. 5, while the absolute shift is shown in Fig. 6. Even after the correction for the telescope drift six of the UVIS full frame filters (F600LP, F631N, F645N, F656N, F775W, and F850LP) show a total offset larger than 0.5 pixels.

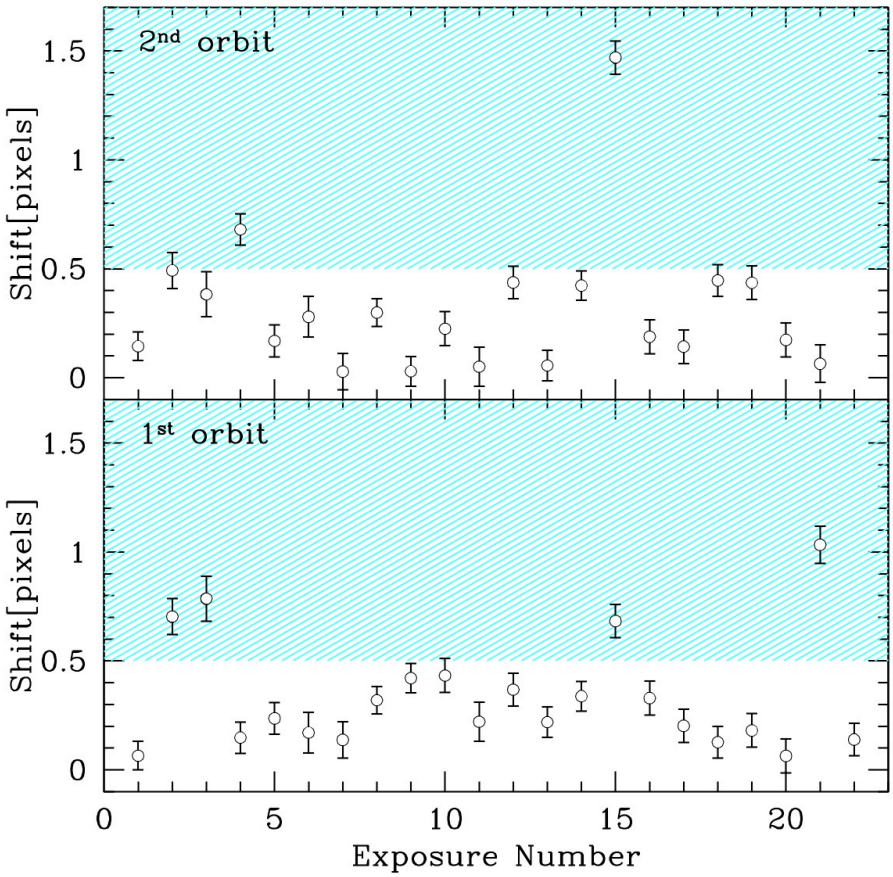

Fig. 6: Absolute positional offset of the stars in NGC1850 once the effect of the telescope drifting is taken into account. The azure shaded area marks the region were CEI specs are not met.

4. Conclusions

The LMC young star cluster NGC 1850 was observed through all the UVIS filters during Cycle 17 as part of the standard WFC3 calibration program (proposal 11923, PI MacKenty). The goal of the proposal was to identify the filters with wedges significant enough to affect those astronomical programs that are sensitive to the relative motion of targets in images taken through multiple filters. Our analysis shows that 36 of the 42 full frame filters of UVIS do not introduce a significant shift in the position of the astronomical sources. However, the filters F600LP, F631N, F645N, F656N, F775W, and F850LP, introduce a shift larger than 0.5 pixels. The filters F600XP and F775W in particular cause a shift larger than 1.0 pixel. The large offset in the F600XP observations was already known from ground-based observations (Baggett et al. 2007), as was the large offset in F775W (Lupie & Boucarut 2003).

References

Baggett, S., Boucarut, R., Tefler, R., Kim Quijano, J., Quijada, M. 2007, *"Performance of the WFC3 Replacement UVIS Filters"*, ISR-WFC3 2007-01

Dressel, L. 2010, *"Wide Field Camera 3 Instrument Handbook, Version 3.0"*, Baltimore: STScI

Gilliland, R.L. 2005, *"Guiding errors in 3-Gyro: Experience from WF/PC, WFPC2, STIS, NICMOS and ACS"*, ISR-Tel-2005-02

Kozhurina-Platais, V., Cox, C., McLean, B., Petro, L., Dressel, L., Bushouse, H., Sabbi, E. 2009, *"WFC3 SMOV Proposal 11444 – UVIS Geometric Distortion Calibration"*, ISR-WFC3-2009-23

Lupie & Boucarut 2003, *"WFC3 UVIS Filters: Measured Troughput and Comparison to Specifications"*, WFC3-ISR 2003-02

Sabbi, E., MacKenty, J., Borders, T. 2010, *"Proposal 11913-IR Filter Wedge Check"*, ISR-WFC3-2010-12

FILTER	X Offset [pix]	Y Offset [pix]	SHIFT [pixels]
F606W	0	0	0
F300X	-0.046±0.065	0.045±0.066	0.065±0.0012
F631N	-0.413±0.078	-0.570±0.087	0.703±0.001
F656N	0.205±0.095	-0.759±0.111	0.786±0.002
F487N	0.024±0.070	-0.146±0.075	0.148±0.001
F502N	-0.153±0.071	-0.189±0.075	0.236±0.001
F200LP	0.087±0.097	0.147±0.090	0.171±0.001
F953N	-0.012±0.079	-0.137±0.087	0.138±0.001
F218W	0.055±0.064	0.315±0.063	0.319±0.001
F225W	-0.094±0.066	0.411±0.070	0.421±0.001
F657N	-0.013±0.074	-0.432±0.082	0.433±0.001
F469N	0.201±0.085	0.091±0.093	0.221±0.001
F336W	0.134±0.074	-0.343±0.076	0.368±0.001
F280N	0.002±0.068	0.219±0.074	0.219±0.001
F343N	-0.292±0.068	0.170±0.068	0.338±0.001
F645N	0.581±0.072	-0.359±0.081	0.683±0.001
F625W	0.309±0.081	0.112±0.076	0.329±0.001
F665N	0.017±0.073	-0.201±0.081	0.202±0.001

F673N	-0.080±0.072	-0.098±0.074	0.127±0.001
F680N	-0.147±0.077	-0.104±0.078	0.181±0.001
F475W	0.063±0.071	0.004±0.086	0.064±0.001
F600LP	-0.426±0.084	0.941±0.088	1.033±0.001
F606W	-0.055±0.076	0.127±0.074	0.139±0.001
F606W	0	0	0
F845M	0.041±0.084	0.138±0.088	0.144±0.001
F555W	-0.229±0.085	-0.436±0.085	0.492±0.001
F814W	-0.235±0.080	-0.302±0.085	0.383±0.001
F850LP	0.077±0.090	-0.676±0.094	0.680±0.002
F689M	0.057±0.077	-0.159±0.074	0.169±0.001
F390M	0.251±0.070	-0.124±0.066	0.280±0.001
F547M	-0.026±0.088	-0.011±0.079	0.028±0.001
F621M	-0104±0.075	0.281±0.069	0.299±0.001
F763M	-0.001±0.076	0.029±0.080	0.029±0.001
F275W	0.111±0.060	0.195±0.068	0.225±0.001
F410M	0.047±0.073	0.018±0.073	0.051±0.001
F467M	0.093±0.070	0.427±0.068	0.437±0.001
F373N	-0.054±0.067	0.014±0.072	0.056±0.001
F438W	-0.115±0.066	-0.407±0.069	0.423±0.001
F775W	0.220±0.077	-1.453±0.077	1.470±0.001
F475X	-0.186±0.083	-0.028±0.081	0.188±0.001
F395N	-0.071±0.066	0.123±0.074	0.142±0.001
F390W	0.161±0.067	-0.417±0.075	0.447±0.001
F350LP	-0.092±0.070	0.426±0.070	0.436±0.001
F658N	0.087±0.085	-0.150±0.091	0.173±0.001
F606W	0.037±0.070	-0.53±0.081	0.064±0.001

Appendix

The maps of the positional offsets with respect to the F606W filters are shown in Figs. 7-16. In each plot the distance is enlarged 20 times.

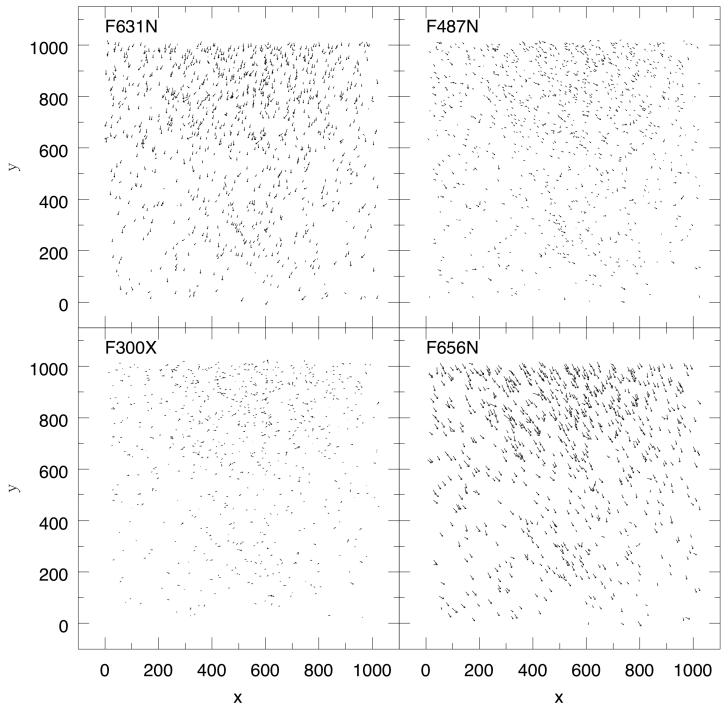

Fig. 7: Shifts of the stars with respect to the F606W filter for the filters F631N, F487N F300X and F656N. Vectors are enlarged 20 times.

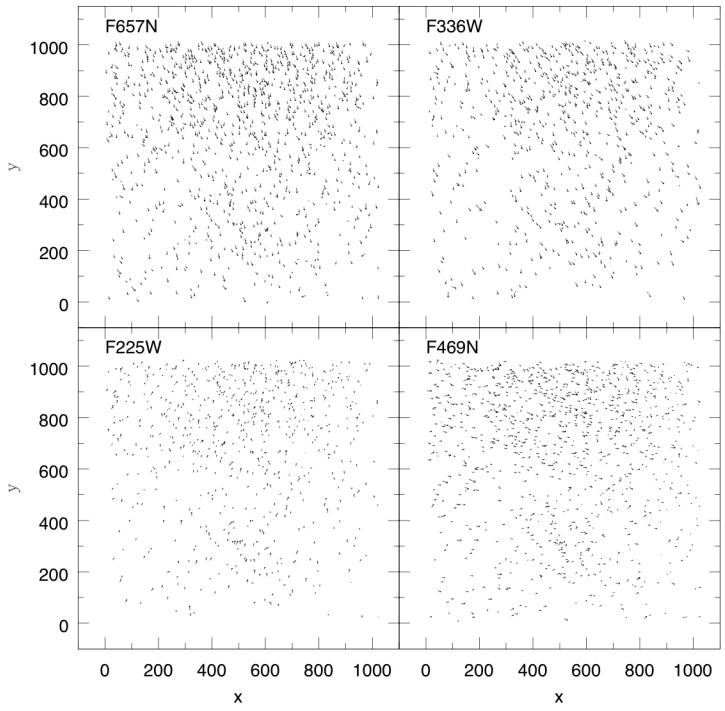

Fig. 8: Same as Fig.7 but for the filters F657N, F336W, F225W, and F469N. Vectors are enlarged 20 times.

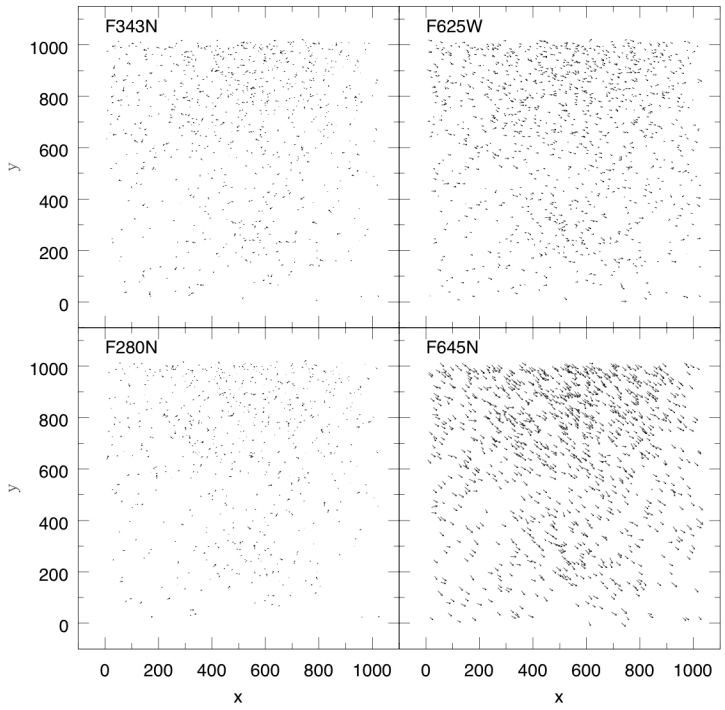

Fig. 9: Same as Fig. 7, but for the filters F343N, F625W, F280N and F645N. Vectors are enlarged 20 times.

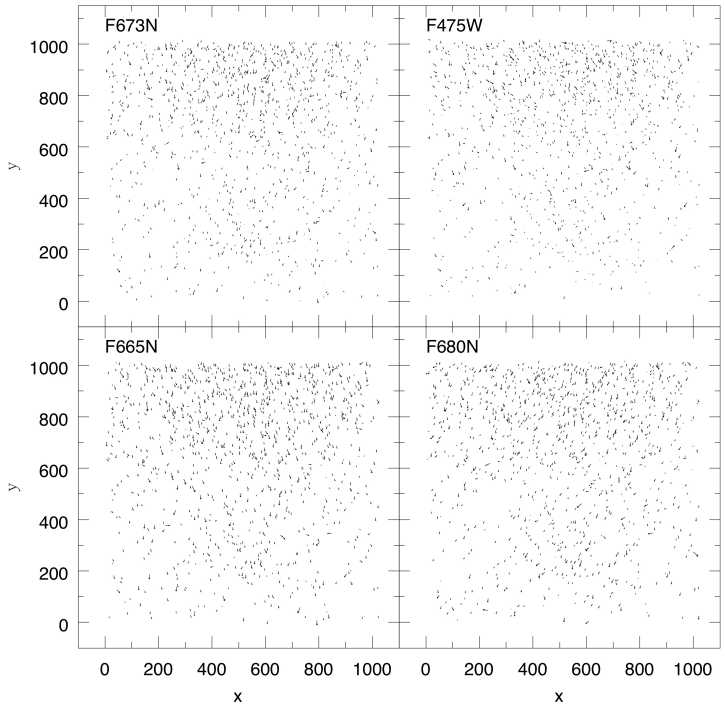

Fig. 10: Same as Fig. 7, but for the filters F673N, F475W, F665N and F680N. Vectors are enlarged 20 times.

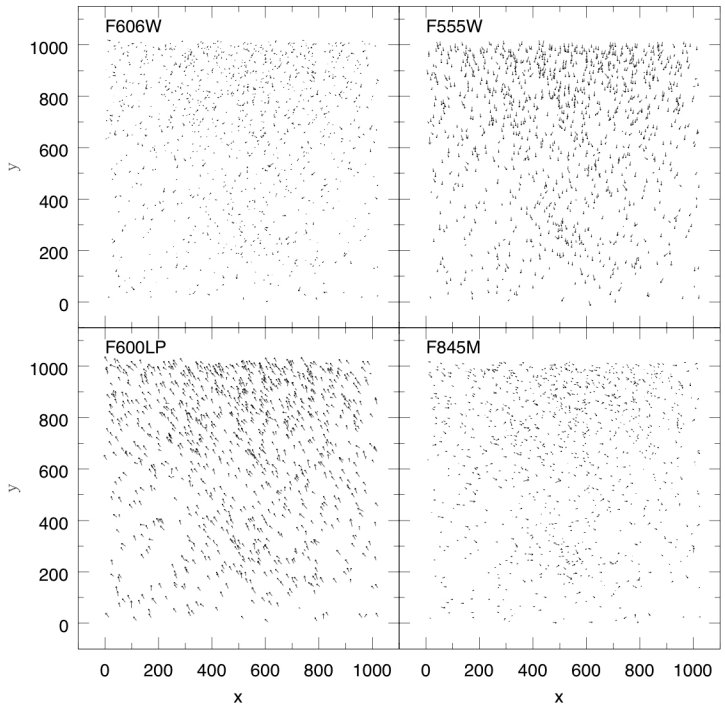

Fig. 11: Same as Fig. 7, but for the filters F606W, F555W, F600LP and F845M. Vectors are enlarged 20 times.

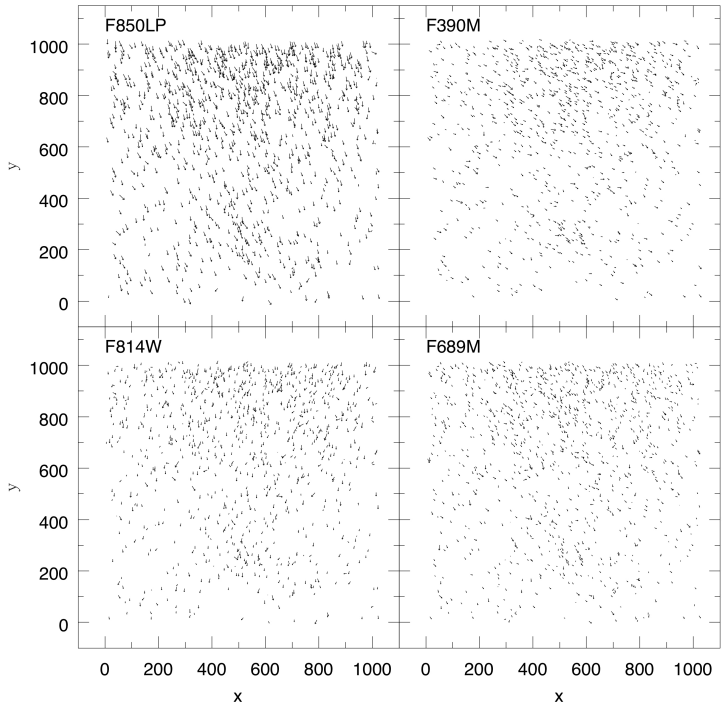

Fig. 12: Same as Fig. 7, but for the filters F850LP, F814W, F390M and F689M. Vectors are enlarged 20 times.

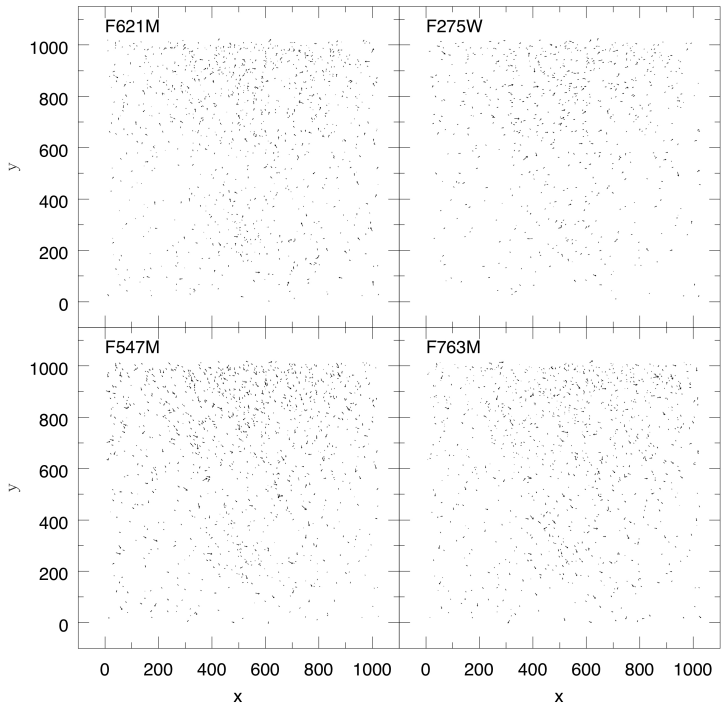

Fig. 13: Same as Fig. 7, but for the filters F621M, F275W, F547M and F763M. Vectors are enlarged 20 times.

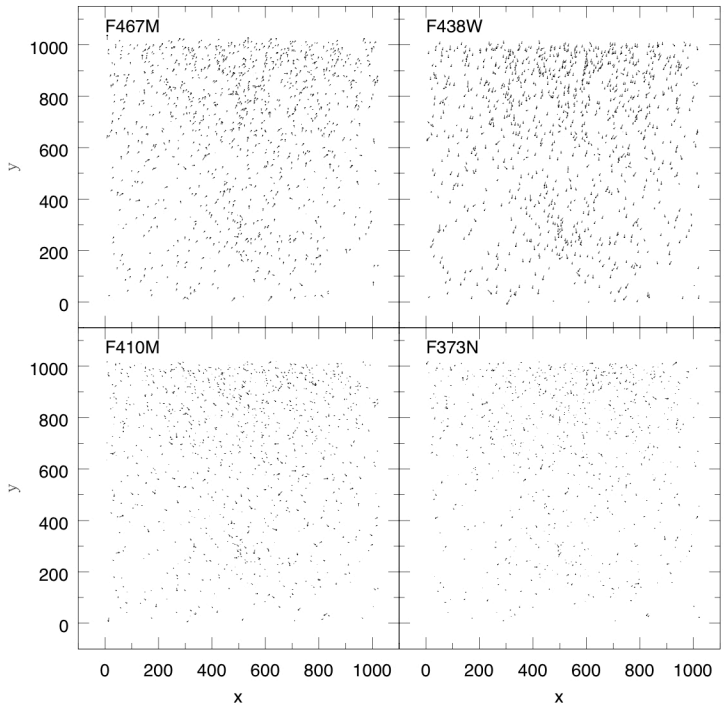

Fig. 14: Same as Fig. 7, but for the filters F467M, F438W, F410M and F373N. Vectors are enlarged 20 times.

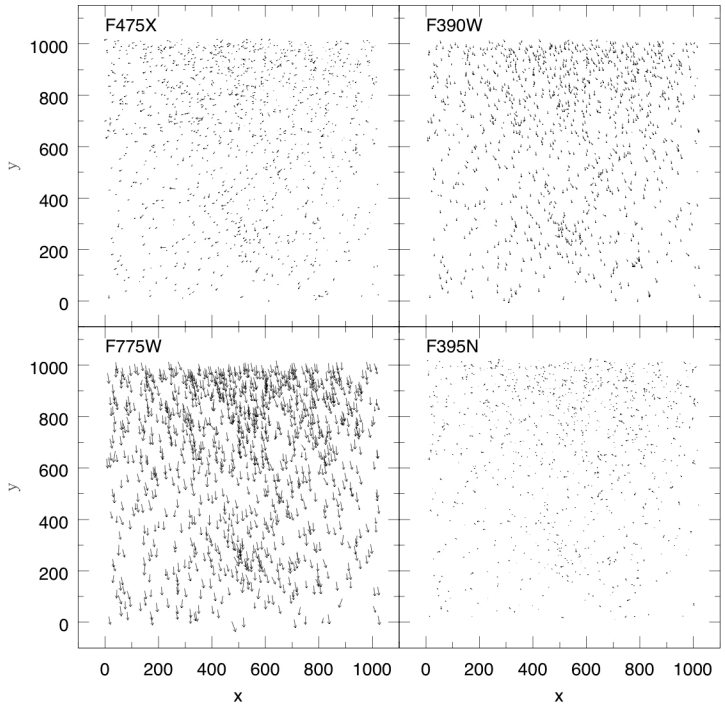

Fig. 15: Same as Fig. 7, but for the filters F475X, F390W, F775W and F395N. Vectors are enlarged 20 times.

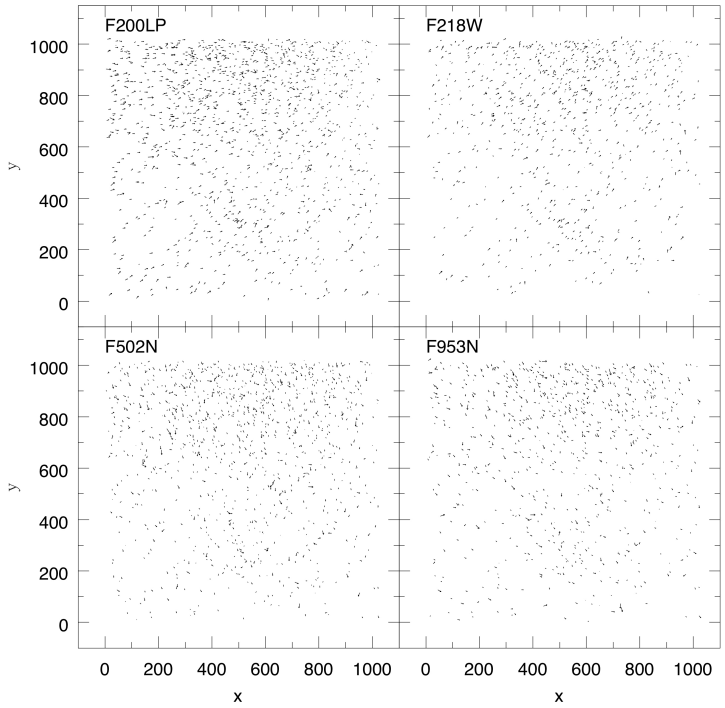

Fig. 16: Same as Fig. 7, but for the filters F200LP, F218W, F502N and F953N. Vectors are enlarged 20 times.